Appl Petrochem Res (2014) 4:55–62
DOI 10.1007/s13203-014-0051-4

KACST FORUM

Ethanol photoreactions over Au–Pd/TiO_2

A. K. Wahab · S. Bashir · Y. Al-Salik · H. Idriss

Received: 6 February 2014 / Accepted: 5 March 2014 / Published online: 21 March 2014

Abstract A prototype Au–Pd/TiO_2 catalyst was prepared, characterized and tested for the photoreaction of ethanol. XPS Au4f and Pd3d indicated that the as-prepared material is composed of metallic Au, metallic Pd as well oxidized Pd (Pd^{2+}). Ar ion sputtering (5 min) of the catalyst surface resulted in almost total reduction of Pd^{2+} to metallic Pd in addition to considerable reduction of surface Ti cations to Ti^{3+} and Ti^{2+} cations; XPS Au4f lines were not affected. Transmission electron microscopic studies indicated that Au particles have a mean particle size of about 3.5 nm while Pd particles are smaller 1–1.5 nm in size. UV excitation of the catalyst in ultrahigh vacuum (UHV) conditions resulted in the formation of acetaldehyde and hydrogen in addition to photodesorption of the reactant ethanol. Hydrogen production, representing ca. 30 % of the desorbing products, was delayed compared to acetaldehyde desorption. This was interpreted as due to kinetic effect whereby initially most electrons transferred to the conduction band are trapped by surface hydroxyls as well inevitable presence of oxygen in the powder accelerating acetaldehyde formation (dehydrogenation). Only once most oxygen-containing species have reacted and molecular hydrogen was formed. To our knowledge, this is the first UHV in situ study of hydrogen production from ethanol photocatalytically over M/TiO_2 system.

Keywords Hydrogen production · Ethanol photoreaction · Gold plasmon · Synergism · Ethanol dehydrogenation

A. K. Wahab · S. Bashir · Y. Al-Salik · H. Idriss (✉)
SABIC-Corporate Research and Innovation (CRI) at KAUST, Thuwal, Saudi Arabia
e-mail: idrissh@sabic.com

Introduction

Light from the sun, the most abundant source of energy on Earth, contributes by <0.05 % of the total power (15,000 GW annual) used by humans (excluding solar heating which contributes around 0.6 %). The estimated practical and convertible power[1] that the Earth surface receives is equivalent to that provided by 600,000 nuclear reactors (one nuclear power plant generates on average 1 GW power). One mode of solar energy utilization is the use of sunlight to generate energy carriers such as hydrogen from renewable sources (e.g., ethanol and water) using semiconductor photocatalysts.

The photo-assisted splitting of water into hydrogen and oxygen was first achieved by Fujishima and Honda [1], who showed that hydrogen and oxygen could be generated in an electrochemical cell containing a titania photoelectrode, provided an external bias was applied. Since that time, numerous researchers have explored ways of achieving direct water dissociation without the need for an external bias. Much work has been conducted since, a large fraction of which is discussed in recent reviews [2–6]. Among the many issues affecting direct water splitting is the need to separate hydrogen from oxygen and the relatively low hydrogen evolution rates so far achieved. These in addition to the need of using UV light (>3 eV) to excite TiO_2 and other related materials has been one of the main obstacles for practical applications. Many authors have sought modified photocatalysts which, unlike pure TiO_2, respond to visible (sunlight) excitation, with limited success to date; see some of these materials in ref. [3].

[1] The total amount of sun light reaching the earth surface is orders of magnitude higher than the quoted figure.

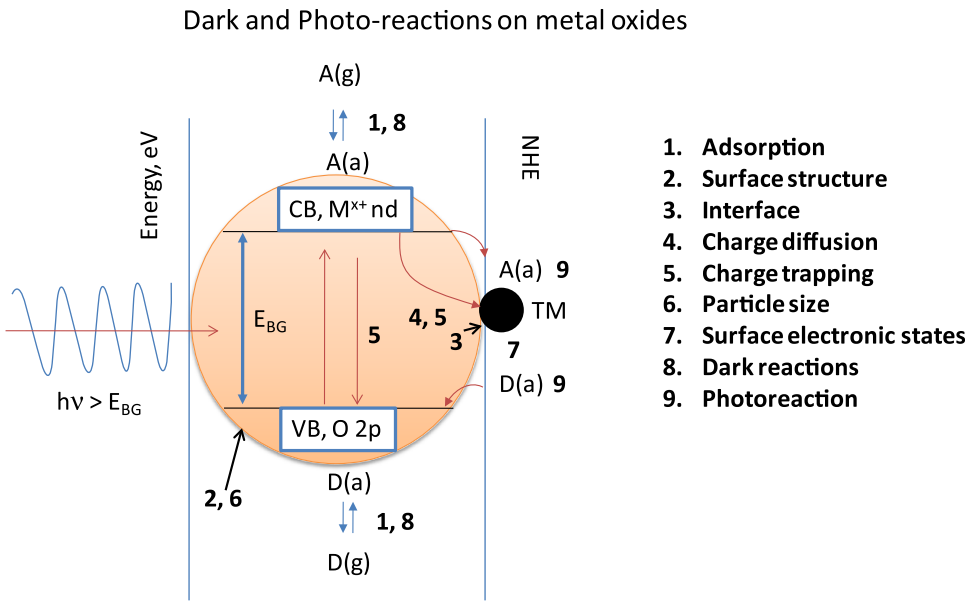

Fig. 1 Schematic representation of the main steps during a photocatalytic reaction involving a metal (*small black circle*) deposited on a metal oxide semiconductor (*large circle*). Also shown are the valence and conduction bands energy with respect to the normal hydrogen electrode (NHE) scale. Adsorbed species are represented by A (electron acceptor) and D (electron donor)

Many approaches have been conducted to design a photocatalyst that can work under direct sunlight in stable conditions. To achieve this, a few key factors need to be overcome chiefs of them are light absorption efficiency, charge carrier life time and materials stability. To enhance light absorption, a large number of photocatalysts were designed based on visible light-range band gap either by solid solutions, hybrid materials or doping of wide-band gap semiconductors. To decrease the charge carriers' life time and also hydride semiconductors, metal nanoparticles are added and sacrificial agents are used [2–6]. The scheme in Fig. 1 presents several steps and concepts involved in photoreactions composed of a semiconductor on which a metal particle is deposited. As can be seen, many factors can affect the reaction in addition to basic thermodynamic requirements and these include charge carrier (electrons and holes) diffusion (step 4) from the bulk to the surface [and interface (step 3)] both affected by bulk and surface structures (step 2) which are in turn related to particle sizes (step 6) and oxidation states (step 7). Kinetics is also important to consider in particular when sacrificial organic compounds are used, therefore, the effect of concentrations and temperatures on the surface populations (step 8) and ultimately the photoreaction rate (step 9) is not negligible [7].

In this work, we present a study on Au–Pd/TiO_2 that is found active for hydrogen production [8]. The Au/TiO_2 system has been studied by us and others in numerous works previously [9–13]. Au metal has at least two important roles in photoreaction, first it acts as sink for transferred electrons from the conduction band and second it contributes by its plasmon response (excited by visible light) in the electron transfer reaction [14–16] albeit is not a fully understood mechanism. To act as an efficient plasmon, Au particles need to be relatively large. Due to this requirement they are less dispersed on the surface of TiO_2. Pd is used to decorate the surface around Au so in essence Pd acts as efficient electron trap center, while Au induces the electric field due to it is electronic oscillation; Pd particles are easily prepared in 1 nm size on top of TiO_2. The TiO_2 used in this work is composed of anatase and rutile phases in ca. 80–20 ratio. This ratio is thought to be in the range where considerable synergism occurs between the two phases further increasing the reaction rate [17]. The catalyst has therefore a combination of properties that are important in photocatalysis: surface plasmons (Au), synergism (anatase + rutile), metal–semiconductor interface (Au/TiO_2 and Pd/TiO_2). In this work, we focus on its properties as well as a mechanistic study of ethanol reaction under UV excitation in which the channels for hydrogen desorption and acetaldehyde desorption seem to be decoupled on the powder material.

Experimental

X-ray photoelectron spectroscopy was conducted using a Thermo scientific ESCALAB 250 Xi. The base pressure of the chamber was typically in the low 10^{-10} to high 10^{-11} mbar range. Charge neutralization was used for all samples. Spectra were calibrated with respect to C1s at 285.0 eV. Au4f, Pd 3d, O1s, Ti2p, C1s and valence band energy regions were scanned for all materials. Typical acquisition conditions were as follows: pass energy = 30 eV and scan rate = 0.1 eV per 200 ms. Ar ion bombardment was performed with an EX06 ion gun at

1 kV beam energy and 10 mA emission current; sample current was typically 0.9–1.0 nA. Self-supported oxide disks of approximately 0.5 cm diameter were loaded into the chamber for analysis. UV–Vis absorbance spectra of the powdered catalysts were collected over the wavelength range of 250–900 nm on a Thermo Fisher Scientific UV–Vis spectrophotometer equipped with praying mantis diffuse reflectance accessory. Absorbance (A) and reflectance (% R) of the samples were measured. The reflectance (% R) data were used to calculate the band gap of the samples using the Tauc plot (Kubelka–Munk function). The TiO_2 exhibited the typical two band gaps of anatase and rutile at 3.2 and 3.0 eV, respectively. BET surface area was measured using Quantachrome Autosorb analyzer by N_2 adsorption. The surface area was found to be 55 m^2/g_{Catal}. Transmission electron microscopy studies were performed at 200 kV with a JEOL JEM 2010F instrument equipped with a field emission source. The microscope was operated in HAADF-STEM mode (Z-contrast). Samples were dispersed in alcohol in an ultrasonic bath and a drop of supernatant suspension was poured onto a holey carbon-coated grid. In situ study was conducted in an ultrahigh vacuum chamber equipped with an online quadrupole mass spectrometer (RGA Hiden; 300 AMU), a sputter ion gun (PHI), a dosing line for ethanol exposure. The chamber is pumped down with an ion pump (PHI), turbo pump (Pfeiffer) and a titanium sublimation pump (PHI). Base pressure was in the low to mid 10^{-9} torr. Catalyst (as a pressed pellet of about 0.5 cm in diameter; total amount about 50 mg) was loaded into an *x*, *y*, *z* R sample mount on top of a Mo sample holder. Prior to reaction the catalyst was cleaned using UV light in presence of 10^{-6} torr of O_2 for 60 min (twice). Ethanol was subjected to freeze–thaw pump to remove residual water and CO_2 and its purity is checked by the online mass spectrometer until a typical ethanol fragment is obtained [18]. Six experiments with different dosing of ethanol were conducted from 90 s to 10 min at a chamber of pressure close to 10^{-7} torr. After dosing, the chamber was pumped down to the 10^{-9} torr range. Prior to UV light form a 100 W ultraviolet lamp (H-144GC-100, Sylvania par 38) with a flux of ca. 10 mW/cm^2 at a distance of 25 cm the sample was rotated away from the mass spectrometer which was turned on to measure the back ground of the chamber. A negligible signal of *m*/*e* 31, the parent ion of the ethanol compared to that of residual N_2/CO (*m*/*e* 28) was indicative of the removal of gas-phase ethanol. The following masses were scanned at a dwell time of 50 ms for each (*m*/*e* 2, 12, 14, 15, 16, 18, 28, 29, 31 and 44) for each run. The catalyst pellet was then turned toward the mass spectrometer which is enveloped with a shroud having an orifice smaller than that of the pellet to minimize stray desorption, at the same time the UV shutter was removed to start the excitation. Au–Pd/TiO_2 (85 % anatase/15 % rutile) catalysts were synthesized by co-impregnation method (0.13 wt% of gold and 0.2 wt% of Pd; 1:3 molar ratio). The precursor of gold and palladium were $AuCl_4$ (dissolved in aqua regia) and $PdCl_2$ in 1 normal HCl. TiO_2 semiconductor, ca. 85 % anatase and 15 % rutile, was used as a support martial. First, TiO_2 was placed into Pyrex beaker. Then, the aqua regia solution of Au and Pd in 1 normal HCl were, respectively, poured into a certain amount of TiO_2 under magnetic stirring (170 rpm) at 80 °C for 12–24 h. The precipitate formed was dried for >4 h, at 120 °C. Finally, the material was calcined at 300 °C for 5 h; afterward it was crushed using a mortar to fine powder.

Results and discussion

Figure 2 presents XPS of the as-prepared Au–Pd/TiO_2 catalyst. Ti2p peaks at 459.2 and 464.6 eV are attributed to the $Ti2p_{3/2}$ and $Ti2p_{1/2}$, respectively. Both the narrow FWHM (1.1 eV) of the $Ti2p_{3/2}$ and the splitting of 5.4 eV are consistent with the presence of Ti^{4+} cations only. O1s peak at 530.3 eV is due to lattice oxygen while the large peak at 532.6 eV is due to irreversibly adsorbed water on the surface; surface hydroxyls at ca. 531.5 eV are masked by the large water contribution. Gold presence can be seen by their XPS Au4f at 83.8 and 87.4 eV attributed to $Au4f_{7/2}$ and $Au4f_{5/2}$, respectively. Both the peak positions and spin splitting of 3.6 eV are characteristic of metallic gold [the 0.2 eV deviation from pure metallic gold (binding energy at 84.0 eV) is slightly larger than the resolution limit and most likely not due to calibration issues]. It has been previously indicated that a charge transfer from TiO_2 to Au results in lowering the binding energy of small metallic particles of Au [19] and this might be the cause. It has also been reported that alloy of Au with Pd results in shifting the Au4f by up to 0.5 eV and at the same time increase in the binding energy of Pd3d by up to 0.8 eV [20]. Also seen in the figure is the contribution of Pd4s lines [because Pd loading is larger (3–1 molar ratio) and their particles are smaller therefore more dispersed; see TEM pictures below]. XPS Pd3d region indicates that Pd exists in two oxidation states, Pd^0 and Pd^{2+}. It is also worth noting that almost at the same binding energy position of Pd3d, Au4d lines are overlapping [21]. However, the signal of Au4d lines is about 5 times weaker than that of Au4f [22]. Given the weak signal of Au4f it is safe to neglect its contribution into the spectrum. The splitting between the XPS $3d_{5/2}$ and $3d_{3/2}$ of both oxidation states of 5.2–5.3 eV is consistent with many other works on both oxidation states [26]. The binding energy of Pd^0 is, however, slightly shifted upward (by 0.3 eV) when compared to Pd metal [20], which may also indicate the presence of some alloy (Au–Pd) (Fig. 3).

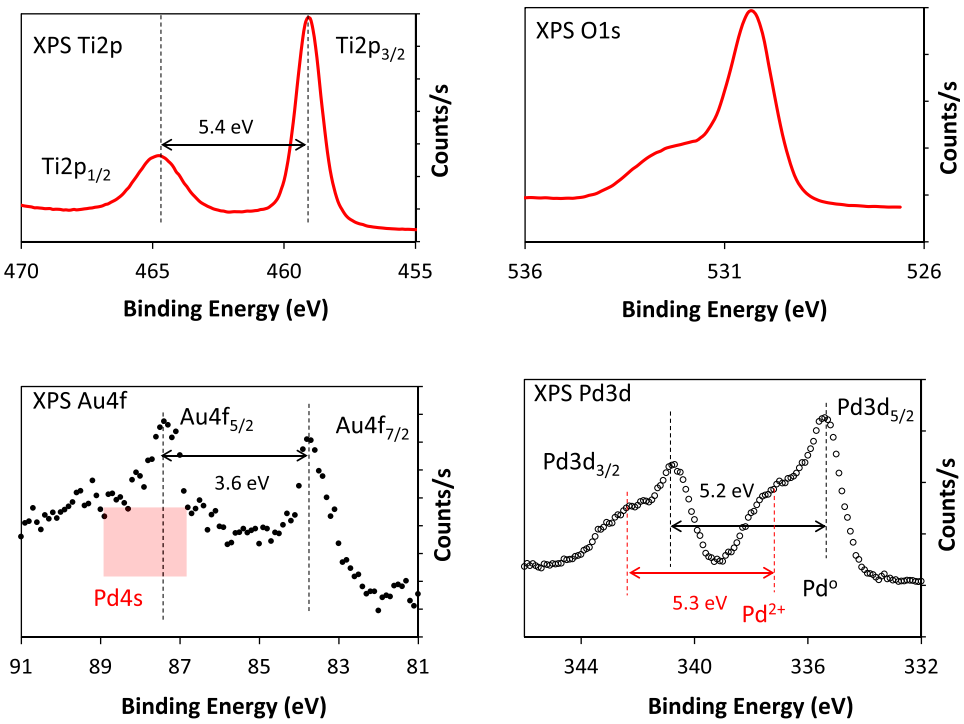

Fig. 2 XPS Au4f, Pd3d, Ti2p and O1s of as-prepared Au–Pd/TiO_2

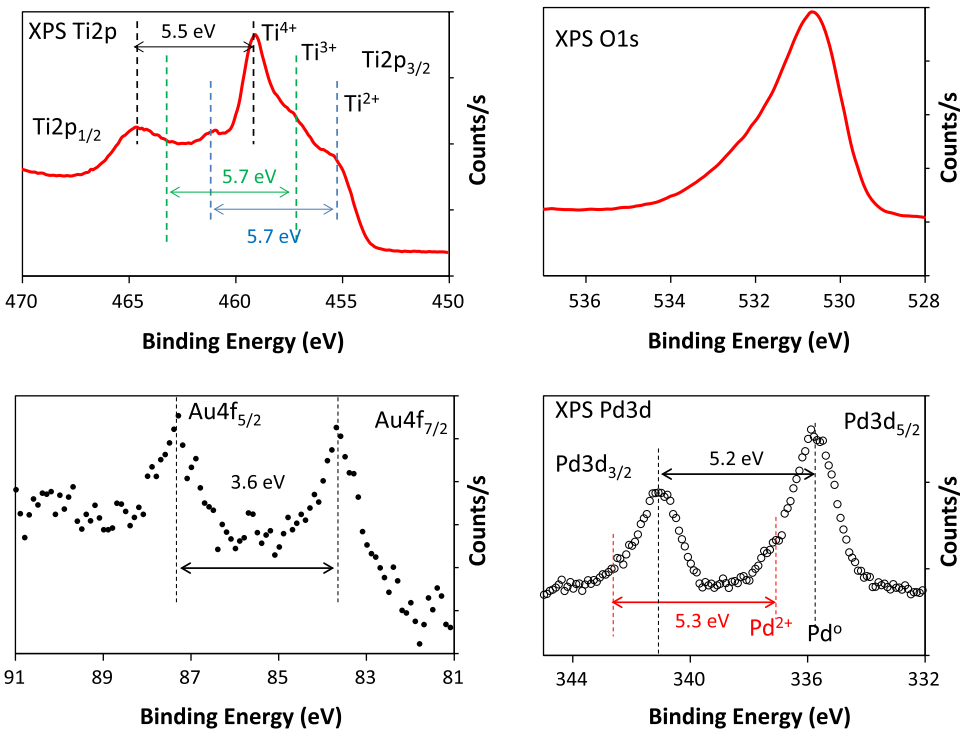

Fig. 3 XPS Au4f, Pd3d, Ti2p and O1s of Ar^+ sputtered sample (5 min) Au–Pd/TiO_2

Figure 2 presents the same lines of Fig. 1 but after Ar^+ sputtering for 5 min to reduce the materials and see for the effect of these on possible electronic shifts. The Ti2p region is that of typical reduced Ti cations (Ti^{4+}, Ti^{3+} and Ti^{2+} and possibly less reduced states with smaller contributions). The XPS $Ti2p_{3/2}$ lines attributed to Ti^{3+} and Ti^{2+} are at 457.3 and 455.3 eV, respectively [23, 24] in agreement with other works. The $Ti2p_{1/2}$ of Ti^{2+} is clear while that of Ti^{3+} is masked by the $Ti2p_{1/2}$ of Ti^{4+} (although one can see a considerable broadening of the peak at the lower binding energy side due to multiple electronic states). The splitting of the three states is very similar (5.5–5.7 eV).

Table 1 XPS surface composition of As prepared and Ar ion reduced Au-Pd/TiO_2

	Area CPS × eV	Sensitivity factor	Corrected area	Atomic (%)
As prepared				
Au4f	222.43	5.24	42.45	0.02
Pd3d	2,423.01	4.64	521.98	0.25
Ti2p	63,711.57	1.80	35,434.69	17.25
O1s	85,127.25	0.71	119,728.90	58.27
C1s	14,724.15	0.30	49,743.75	24.21
Ar^+ sputtered				
Au4f	178.04	5.24	33.98	0.02
Pd3d	1,195.65	4.64	257.57	0.14
Ti2p	76,212.77	1.80	42,387.53	22.44
O1s	64,737.00	0.71	91,050.63	48.20
C1s	16,327.96	0.30	55,162.03	29.20

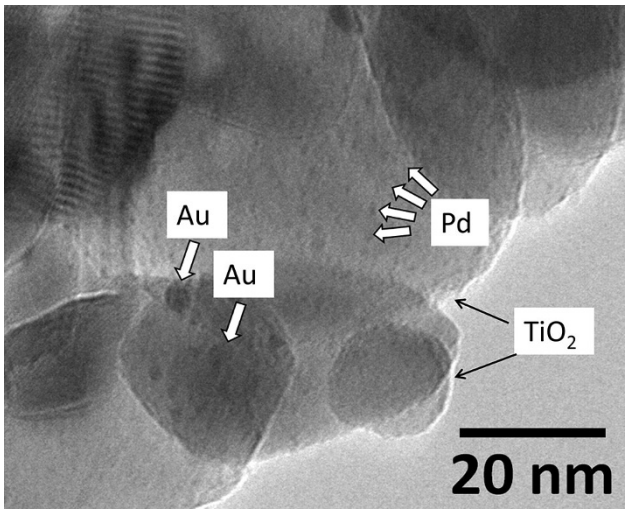

Fig. 4 Transmission electron microscopy of Au/Pd TiO_2 (anatase + rutile)

The O1s region also has the typical reduced shape as seen by Doniac broadening at the high binding energy side [25]. The XPS Au4f region has changed slightly also the background appeared to be less prominent probably because of a more homogenous electronic distribution of Pd particles (contributing by their 4s into the spectrum). The XPS Pd3d indicates that most of Pd particles are now in their reduced state. Both XPS Au4f and 3d main peak positions did not change considerably upon Ar ion sputtering. Table 1 presents the atomic % of the Au–Pd/TiO_2 before and after Ar ions sputtering.

In Fig. 4 a representative transmission electron microscopy image of the Au–Pd/TiO_2 catalyst. A large number of images were collected. The mean particle size of Au is about 3.5 nm while that of Pd is 1.5 nm (although the Pd particle size distribution was asymmetric at the low size

Table 2 Photoreaction for hydrogen production from water in presence of 5 vol% of organic sacrificial agent in water (ethylene glycol in the case of Pd/TiO_2 and Au–Pd/TiO_2 and ethanol in the case of Au/TiO_2—both sacrificial agents are very efficient for the hole capturing with slight variations (ca. 10 %)

Catalyst	Rate (mol/g_{Catal} min)
0.15 at.% Pd/TiO_2	2.3×10^{-5}
0.20 at.% Au/TiO_2	1.7×10^{-4}
0.05 at.% Au–0.15 at.% Pd/TiO_2	2.8×10^{-4}

Amount of catalyst = 25 mg; reactor volume 100 mL, light Hg mercury lamp with 360 nm cutoff filter. Flux ca. 4–5mW/cm^2 (comparable to that provided from the sun in summer midday at a longitude = 25°N)

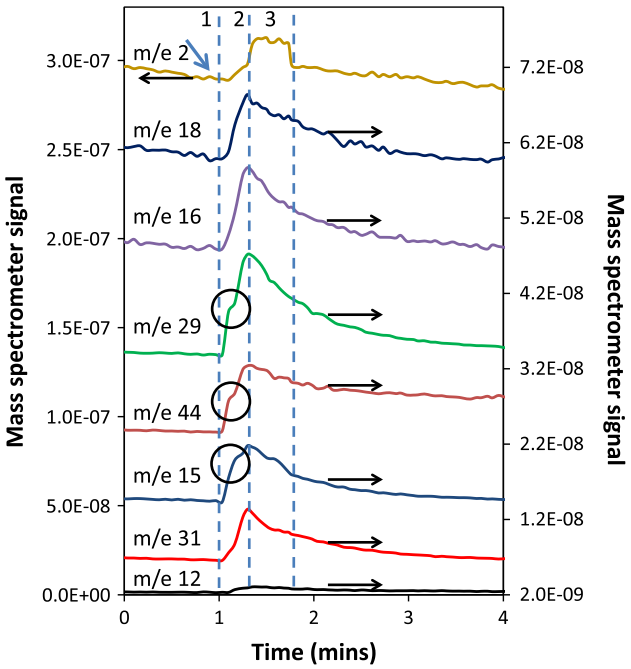

Fig. 5 Mass spectrometer fragmentation pattern of products collected upon ethanol photoreaction under UV excitation for a previously exposed Au–Pd/TiO_2 to ethanol for 4 min at 10^{-7} torr (this exposure was found to ensure surface saturation based on monitoring of desorption products)

indicating a larger contribution of small particles <1 nm); there was negligible number of Pd particles above 2 nm. The TEM images of the anatase and rutile phases of this TiO_2 have been presented elsewhere; the difference between the two phases can be made based on their local diffraction lines as well as the lattice spacing from high-resolution images.

Table 2 presents the rate of reaction for hydrogen production for Pd/TiO_2, Au/TiO_2 and Pd–Au/TiO_2. The support (85 % anatase/15 % rutile) was the same for the three catalysts. It is to be noted that variations from preparations to the other may contribute by up to 25 % of changes in the

Table 3 CF for mass spectrometer correction factor

m/e	Peak area	Product	CF	Peak area	Selectivity (%)
2	6.9×10^{-7}	Hydrogen	0.5	3.5×10^{-7}	29.4
12	1.1×10^{-8}				
15	5.9×10^{-8}				
16	1.9×10^{-7}				
18	1.7×10^{-7}	Water	1.1	1.9×10^{-7}	15.9
29	2.6×10^{-7}	Acetaldehyde	2.1	5.5×10^{-7}	46.5
31	5.4×10^{-8}	Ethanol	1.8	9.7×10^{-8}	8.3
44	1.2×10^{-7}		1.2		
Total	1.6×10^{-6}			1.2×10^{-6}	

reaction rate and that the rate is dependent on the % of the metal in a non-correlated way as often observed (see for example ref. [12]). Still it is clear that the catalyst composed of Pd–Au/TiO_2 is more active than that from Au/TiO_2 and Pd/TiO_2. A similar observation was reported on Pt–Au/TiO_2 previously [26].

To analyze the reaction products and their evolution with time upon radiation we have opted to conduct experiment in which the photocatalyst is illuminated with online mass spectrometer. Figure 5 presents the UV-excited photoreaction over Au–Pd/TiO_2 that was initially saturated with ethanol (prior to excitation). Upon illumination (indicated by the thick arrow at the top of the figure) fragments of reaction products are observed to desorb followed by a decrease in the signal due to surface depletion of the reactant. The desorption of these products can be grouped in three modes: photodesorption, photoreduction and photooxidation. Ethanol adsorption on TiO_2, as well as M/TiO_2 (M = Au, Pd or both) at room temperature gives both molecular and dissociated species. This has been seen both experimentally [27] and by DFT computation methods [28]. As indicated in Fig. 2, the surface contains (in addition to ethanol) non-negligible amounts of irreversibly adsorbed water and these ultimately give hydroxyl radicals upon photoexcitation. There are three regions in the figure denoted by lines 1, 2 and 3. In region 1–2, desorption of all products occurs (except hydrogen). In addition, this desorption is different for the set of products monitored. Ethanol (*m/e* 31), water (*m/e* 18) and oxygen (*m/e* 16; *m/e* 32 has the same desorption profile) all have similar shape and these may be considered as due to photodesorption upon UV excitation. In addition, fragments related to acetaldehyde are clearly noticed (*m/e* 29 and *m/e* 44). *m/e* 29 is largely due to acetaldehyde (CHO) fragment as ethanol contribution into this fragment is small (typically <30 % of *m/e* 31). *m/e* 44 (parent acetaldehyde molecule) has contribution from CO_2 in addition. The ratio *m/e* 29 to *m/e* 44 of about 5–2 indicates that in this region most of desorption is due to acetaldehyde [29]. *m/e* 15 (CH_3) has contribution from both acetaldehyde and ethanol. Seen in this region is a clear shoulder (indicated by a circle) composed of these three masses only. This is a clear indication of acetaldehyde desorption due to ethanol dehydrogenation. The formation of acetaldehyde from ethanol over TiO_2 upon photoreaction in presence of oxygen on TiO_2 single crystal has been reported before [27]. The reaction that involves two-electron injections into the valence band can be explained as follow.

Dissociative adsorption of ethanol and water occurs on the surface of TiO_2 in the presence or absence of light.

$$CH_3CH_2OH + Ti^{4+} - O_s^{2-} \rightarrow CH_3CH_2O - Ti^{4+} + OH(a) \quad (1)$$

$$H_2O + Ti^{4+} - O_s^{2-} \rightarrow HO - Ti^{4+} + OH(a) \quad (2)$$

s for surface, (a) for adsorbed.

Light excitation of the catalyst resulting in electron (e^-)–hole (h^+) pair formation.

$$TiO_2 + nUV \rightarrow xe^- + xh^+ \quad (3)$$

where $n > x$ due to scattering and absorption cross section.

Hole scavenging (two electrons injected per ethoxide into the VB of TiO_2) followed by acetaldehyde formation.

$$CH_3CH_2O - Ti_s^{4+} - O_s^{2-} + 2\,h^+ \rightarrow CH_3CHO\,(g) + OH(a) + Ti_s^{4+} \quad (4)$$

On average, acetaldehyde maximum separate desorption (in region 1–2) occurred after 3 s from UV excitation. The maximum desorption is, however, seen together with ethanol and water desorption at about 20 s of light excitation. In region 2–3, all products start to decrease but hydrogen desorption increased reached a short plateau before a sharp decrease. The observed profile can be rationalized kinetically and due to diffusion. Initially the surface contains large amounts of adsorbed ethanol but also adsorbed water and irreversibly adsorbed O_2 molecules (in the sample cleaning process). Upon illumination, the initial reaction is photooxidation producing acetaldehyde. The formation of acetaldehyde can, if coupled to oxygen radical species, prevent the reduction of H ions because O_2 is a faster electron scavenger. Once a large fraction of oxygen atoms and molecules have been consumed the remaining ethanol and water could farther react with the generated holes. Electrons transferred to the conduction band can then be transferred to Au and Pd particles that in turn reduce hydrogen ions (of surface hydroxyls) to molecular hydrogen; as follow [considering Eqs. (1)–(4) above].

Electron transfer from the CB of TiO_2 to H^+ (via M nanoparticles) resulting in molecular hydrogen formation, while the hole transfer occurs from one OH species of water in addition.

$$4\ OH\ (a) + 4\ e^- + 2\ h^+ \rightarrow 3O_s^{2-} + 1/2\ O_2 + 2\ H_2 \quad (5)$$

Because of the small size of hydrogen ions, intra and inter diffusion is much faster than for ethanol, acetaldehyde and water, is a plausible explanation of the abrupt decrease of the signal. The signal of all, but *m/e* 44 products return to the base line. The remaining *m/e* 44 signal is due to total oxidation of traces of ethanol to CO_2 (as it is not mirrored by *m/e* 29 and *m/e* 15; fingerprint of acetaldehyde); it is worth indicating that photooxidation of ethanol is a set of consecutive reactions studied in some details previously on TiO_2 [30] as well as on Ru/TiO_2 [31].

Table 3 presents the computed peak areas of the mass spectrometer signals of the main products. In addition, the corrected peak areas, to the mass spectrometer sensitivity factors for hydrogen, water, ethanol and acetaldehyde are given. While the results are preliminary it is, however, clear that hydrogen desorption contributes by a non-negligible fraction of the overall desorption and that acetaldehyde represents the largest fraction. In the absence of molecular oxygen one would expect that the amount of hydrogen would be at least equal to that of acetaldehyde if all hydrogen is made from ethanol and would be larger if additional hydrogen is made from adsorbed water.

Conclusions

$Au–Pd/TiO_2$ catalysts combining both plasmonic and synergism behavior are prepared, characterized and tested for the photoreaction of ethanol under ultrahigh vacuum condition upon excitation with UV light. The catalyst is composed of metallic Au and Pd in their reduced state. The photoreaction of ethanol results in the production of acetaldehyde and hydrogen. Hydrogen production is retarded due to the initial reaction of surface hydroxyls and adsorbed oxygen atoms and or molecules. Only once most of these species were consumed and molecular hydrogen was formed.

References

1. Fujishima A, Honda K (1972) Electrochemical photolysis of water at a semiconductor electrode. Nature 238:37
2. Kudo A, Miseki Y (2009) Heterogeneous photocatalyst materials for water splitting. Chem Soc Rev 38:253
3. Connelly KA, Idriss H (2012) The photoreaction of TiO_2 and Au/TiO_2 single crystal and powder surfaces with organic adsorbates. Emphasis on hydrogen production from renewable. Green Chem 14:260–280
4. Nadeem MA, Connelly KA, Idriss H (2012) The photoreaction of TiO_2 and Au/TiO_2 single crystal and powder with organic adsorbates. Int J Nanotechnol (special edition on nanotechnology in Scotland) 9:121–162
5. Connelly KA, Wahab AK, Idriss H (2012) Photoreaction of Au/TiO_2 for hydrogen production from renewables: a review on the synergistic effect between anatase and rutile phases of TiO_2. Mater Renew Sustain Energy 1:1–12
6. Walter MG, Warren EL, McKone JR, Boettcher SW, Mi Q, Santori EA, Lewis NS (2010) Solar water splitting cells. Chem Rev 110:6446–6473
7. Yang YZ, Chang CH, Idriss H (2006) Photo-catalytic production of hydrogen from ethanol over M/TiO_2 catalysts (M = Pd, Pt or Rh). Appl Catal B: Environ 67:217–222
8. Wahab AK, Al-Oufi M, Bashir S, Al-Salik Y, Katsiev H, Idriss H (2013) Photocatalyst, method of preparation, photolysis system. World Patent 13T&I0037-WO-PCT (2013); Gulf Cooperation Council (13T&I0037-GC-NP), Serial Number GCC/P/2013/25576 International Procedure (13T&I0037-WO-PCT), Serial Number PCT/IB13/59406
9. Jovic V, Al-Azria ZHN, Sun-Waterhouse D, Idriss H, Waterhouse GIN (2013) Photocatalytic H_2 production from bioethanol over Au/TiO_2 and Pt/TiO_2 photocatalysts under UV irradiation—a comparative study. Top Catal 56:1139–1151
10. Waterhouse GIN, Wahab AK, Al-Oufi M, Jovic V, Anjum DH, Sun-Waterhouse D, Llorca J, Idriss H (2013) Hydrogen production by tuning the photonic band gap with the electronic band gap of TiO_2. Scientific Rep 3:1–5
11. Jovic V, Chen WT, Blackford MG, Idriss H, Waterhouse GIN (2013) Effect of gold loading and TiO_2 support composition on the activity of Au/TiO_2 photocatalysts for H_2 production from ethanol–water mixtures. J Catal 305:307–317
12. Bowker M, Millard L, Greaves J, James D, Soares J (2004) Photocatalysis by Au nanoparticles: reforming of methanol. Gold Bull 37:3–4
13. Subramanian V, Wolf EE, Kamat PV (2004) Catalysis with TiO_2/gold nano composites: effect of metal particle size on the fermi level equilibration. J Am Chem Soc 126:4943–4950
14. Du L, Furube A, Yamamoto K, Hara K, Katoh R, Tachiya M (2009) Plasmon-induced charge separation and recombination dynamics in gold TiO_2 nanoparticles systems: dependence on TiO_2 particle size. J Phys Chem C 113:6454–6462
15. Seh ZW, Liu S, Low M, Zhang SY, Liu Z, Mlayah A, Han MY (2012) Janus Au–TiO_2 photocatalysts with strong localization of plasmonic near-fields for efficient visible-light hydrogen generation. Adv Mater 24:2310–2314
16. Zhang Z, Zhang L, Hedhili MN, Zhang H, Wang P (2013) Plasmonic gold nanocrystals coupled with photonic crystal seamlessly on TiO_2 nanotube photoelectrodes for efficient visible light photoelectrochemical water splitting. Nano Lett 13:14–20
17. Bashir S, Wahab AK, Idriss H (2014) Synergism and photocatalytic water splitting to hydrogen over Pt/TiO_2 catalysts: effect particle size. Catal Today (submitted)
18. http://webbook.nist.gov/Massfragmentationethanol
19. Kruse N, Chenakin S (2011) XPS characterization of Au/TiO_2 catalysts: binding energy assessment and irradiation effects. Appl Catal A 391:367–376
20. Yi CW, Luo K, Wei T, Goodman DW (2005) The composition and structure of Pd–Au surfaces. J Phys Chem B 109:18535
21. Li Z, Gao F, Wang Y, Calaza F, Burkholder L, Tysoe WT (2007) Formation and characterization of Au/Pd surface alloys on Pd (111). Surf Sci 601:1898–1908

22. Moulder JF, Stickle WF, Sobol PE, Bomben KD (1992) Handbook of X-ray photoelectron spectroscopy, Perkin-Elmer Corporation
23. Idriss H, Barteau MA (1994) Reactions of p-benzoquinone on TiO_2(001) single crystal: oligomerization and polymerization by reductive coupling. Langmuir 10:3639–3700
24. Idriss H, Barteau MA (1994) Characterization of TiO_2 surfaces active for novel organic synthesis. Catal Lett 26:123–139
25. Doniach S, Sunjic M (1970) Many-electron singularity in X-ray photoemission and X-ray line spectra from metals. J Phys C Solid 3:285
26. Montini T, Marelli M, Minguzzi A, Gombac V, Psaro R, Fornasiero P, DalSanto V (2012) H_2 production by renewables photoreforming on Pt–Au/TiO_2 catalysts activated by reduction. ChemSusChem 5:1800–1811
27. Nadeem MA, Murdoch M, Waterhouse GIN, Metson JB, Keane MA, Llorca J, Idriss H (2010) Photoreaction of ethanol on Au/TiO_2 anatase. Comparing the micro to nano particle size activities of the support for hydrogen production. J PhotoChem PhotoBiol A: Chem 216:250–255
28. Muir JN, Choi YM, Idriss H (2012) DFT study of ethanol on TiO_2 (110) rutile surface. Phys Chem Chem Phys 14:11910–11919
29. Idriss H, Kim KS, Barteau MA (1993) Carbon–carbon bond formation via aldolization of acetaldehyde on single crystal and polycrystalline TiO_2 surfaces. J Catal 139:119–133
30. Reztova T, Chang C-H, Koersh J, Idriss H (1999) Dark and photoreactions of ethanol and acetaldehyde over TiO_2/carbon molecular sieve fiber. J Catal 185:223–235
31. Kundu S, Vidal AB, Nadeem A, Senanayake SD, Stacchiola D, Idriss H, Rodriguez J (2013) Ethanol photo reaction on ruthenium metal/metal oxide modified rutile TiO_2 (110) single crystal surface. J Phys Chem C 117:11149–11158